RESEARCH MEMORANDUM

A SUMMARY REPORT ON THE EFFECTS OF MACH NUMBER

ON THE SPAN LOAD DISTRIBUTION ON

WINGS OF SEVERAL MODELS

By Henry Jessen, Jr.

Ames Aeronautical Laboratory
Moffett Field, Calif.

NATIONAL ADVISORY COMMITTEE
FOR AERONAUTICS

WASHINGTON

July 15, 1947

NACA RM No. A7C28

NATIONAL ADVISORY COMMITTEE FOR AERONAUTICS

RESEARCH MEMORANDUM

A SUMMARY REPORT ON THE EFFECTS OF MACH NUMBER ON THE SPAN LOAD DISTRIBUTION ON WINGS OF SEVERAL MODELS

By Henry Jessen, Jr.

SUMMARY

The change in spanwise load distribution at high Mach numbers is of considerable interest because lateral movement of the center of lift affects the trim, stability, and structural factors of safety of an airplane. The effects of Mach number upon the span load distribution of various airplanes have been predicted from the results of several series of model tests in high-speed wind tunnels, but all tests were not made under comparable conditions. Different model support struts were used and various methods of tunnel calibration were employed. Furthermore, the results of the various tests were not presented in the same manner. This report is an attempt to correlate these data by reducing them to similar test conditions and parameters.

Although the available data are too meager to permit isolation of the effects of changes in wing configuration, in a majority of cases the tests reveal a tendency for the center of lift to shift outboard with increasing Mach number. The exceptions noted are a wing with a thickened and swept-back root section which housed an air-inlet duct, and a highly tapered wing of constant thickness ratio with about 2° of washout.

The theoretical span load distribution was computed and compared with the wind-tunnel results for the two cases where high-speed airfoil section data were available and the agreement was quite satisfactory.

INTRODUCTION

Most high-speed airplanes attain velocities even in shallow dives great enough to cause the critical Mach number of the wing to be exceeded. As the critical Mach number usually varies across the span of the wing due to changes in wing profile and thickness, or to the presence of nacelles, local sweepback, and fuselage interference, the load distribution may be strongly affected by compressibility. If the center of lift shifts outboard, the bending moment in the wing root may become large enough to cause structural failure. Although several series of high-speed span-load investigations have been made during recent years, the results are not readily comparable because the models represented widely different types of airplanes and were tested on various support systems. All basic data in this report are from tests in the Ames 16-foot high-speed wind tunnel except those of the high-aspect-ratio wing which are from tests in the Langley 8-foot high-speed wind tunnel. As improved methods of calibrating wind tunnels and computing constriction corrections were developed, they were incorporated into the test procedures. Finally, the results of the tests were presented in various ways so direct comparisons of the data were difficult. Since this report is merely a summary of the results of tests of the unrelated models previously mentioned and includes no further investigations in which the effects of the variables were systematically determined, most of the deficiencies of the original results still exist. However, all data have been reduced to the same parameters and the same constriction and calibration factors have been applied where possible.

MODEL AND APPARATUS

The models tested in the Ames 16-foot wind tunnel were three-dimensional models of complete airplanes and were mounted on two front struts and a tail strut. A sketch showing plan and front views of the left half of each model, the location of the front support struts, and a table of basic data are included in figures 1 through 7. The front support struts for the model of figure 6 were so arranged that the leading edges of the struts were at the trailing edge of the wing. These struts had a thickness-to-chord ratio of 0.12 and most of each strut was covered with a fairing. For the other Ames tests the front support struts had a thickness-to-chord ratio of 0.05 and chords of 8 inches at the model and 60 inches at the tunnel wall. The rear strut had a thickness-to-chord ratio of 0.07 and a 20-inch chord. All three struts were used without fairings.

The high-aspect-ratio wing model (fig. 1) tested in the Langley 8-foot high-speed wind tunnel was mounted on a thin vertical plate on the model and tunnel center line.

The locations of rows of wing pressure orifices are indicated by dashed lines on the sketches of the models.

REDUCTION AND ANALYSIS OF DATA

Symbols

The symbols used in this report are defined as follows:

A	aspect ratio (b^2/S)
a	speed of sound in free stream, feet per second
b	span of wing, feet
C_L	lift coefficient (L/qS)
c	section chord of model, feet
$\bar{c}$	mean model chord (S/b), feet
c_n	section normal-force coefficient (n/qc)
g	acceleration equal to gravity, 32.2 feet per second per second
L	lift on model, pounds
M	Mach number (V/a)
M_{cr}	critical Mach number (free-stream Mach number at which the local velocity becomes sonic)
n	section normal force, pounds / FT
q	dynamic pressure in free stream, pounds per square foot ($\frac{1}{2}\rho V^2$)
S	area of wing, square feet
V	velocity of free stream, feet per second
y	distance along semispan from center line of symmetry, feet

α angle of attack of wing chord line or fuselage reference line (see figs. 1 to 7), corrected for tunnel-wall effects and upflow, degress

ρ mass density in free stream, slugs per cubic foot

Methods of Reduction

In every case the pressure-distribution data were reduced to section normal-force coefficients by integration of curves giving the upper and lower surface pressure coefficients along the chord of each section. No corrections for wing dihedral were made to the section loading coefficients $c_n c/\bar{c}$ when they were plotted along the model span. The centroids of the loading were determined by integration of curves of section loading coefficients plotted along the span.

The lateral centers of lift were determined by integrating the loading curves shown in figures 1 to 7 without extrapolating the curves inboard of the points at which the data terminate. Therefore, the lateral centers of lift shown are actually the centroids of the loading outboard of the pressure stations at which the loading curves terminate and show the effects of Mach number upon the bending moment at these stations rather than at the actual wing root.

Methods of Analysis

In this report the theoretical loading was computed by a generalized method of applying lifting-line theory (reference 1) which utilizes actual high-speed wind-tunnel data. Most previous reports on span-load tests presented a theoretical loading computed by the method of ANC-1(1) (reference 2) using experimental or estimated low-speed airfoil characteristics.

RESULTS AND DISCUSSION

The Ames 16-foot wind-tunnel tests summarized in this report cover a Mach number range of 0.40 to 0.80 or 0.825 and the Langley 8-foot wind-tunnel tests extend from a Mach number of 0.40 to 0.925. The Reynolds number for the Ames tests varies from 4,000,000 for the smallest model at 0.40 Mach number to 9,000,000 for the largest model at 0.80 Mach number. Reynolds numbers of 900,000 at a Mach number of 0.4 and 1,400,000 at 0.90 Mach number were attained during

the Langley tests.

The variation of critical Mach number along the model span is shown in figure 8 for several of the models tested. Models A and C show the normal variation, the thicker root sections having the lower critical Mach numbers. Quite the reverse is true in the case of model B where the inboard section has the highest critical Mach number except at negative or large positive lift coefficients when the pressures reach critical values over the duct lip. This unique effect appears to be the result of several factors. When air is flowing through the duct a higher critical Mach number is maintained over a wider range of lift coefficients than when the ducts are closed. Even with the ducts closed, however, the root section has a higher critical Mach number than an NACA 66-series airfoil of comparable thickness-to-chord ratio; so it is obvious that the excellent high-speed characteristics are due in part to three-dimensional effects produced by the marked sweepback and taper existing over this portion of the wing. Model D has a relatively small variation in critical Mach number across the wing span, the root and tip sections having somewhat higher values for all lift coefficients up to about 0.70. A somewhat similar variation of critical Mach number exists across the span of model E. The tip sections always have the highest critical Mach number and the middle portions of the wing have the lowest. The slight increase in critical Mach number at the point of dihedral reversal (approximately 0.4 semispan) for lift coefficients of 0.60 and 0.80 is probably due to local separation and the reduced lift coefficient occurring at this point.

Lift Characteristics

The variation of the lift-curve slopes and angles of zero lift with Mach number is shown in figure 9. In every case the lift-curve slope increases smoothly up to some Mach number between 0.675 and 0.775 and then breaks sharply downward. This Mach number of divergence varies with the wing thickness, the break in the curve occurring at the lower Mach numbers for the thicker wings. The angle of attack for zero lift remained constant or decreased slightly up to about 0.70 Mach number for all models. With further increases in Mach number the zero-lift angle of models B, D, and E shifted abruptly in a positive direction, while the increases for models C and F were more gradual. Up to 0.80 Mach number the zero-lift angles of Model A and the high-aspect-ratio wing had changed only about 0.5° although the high-aspect-ratio wing experienced a rather large increase above 0.825 Mach number and

it appeared that model A might do likewise at the higher Mach numbers. Model B experienced the largest increase in zero-lift angle, the shift being nearly 4° between Mach numbers of 0.40 and 0.80.

Span Load Distribution

As the models for which high-speed span-load data are available vary widely in general configuration, airfoil section, thickness and twist distribution, plan form, and aspect ratio, it is not possible to isolate the effects of these variables. Theoretical analysis of the loading is further complicated by the fact that most models employed modified airfoil sections for which no high-speed section data were available. Consequently, all that could be done was to reduce the original data to similar test conditions and to the same loading coefficients and to present it at the same values of angle of attack and Mach number.

Although the low-speed span loading can usually be predicted with reasonable accuracy using the method of ANC-1(1) (reference 2), this procedure is of little value for high-speed conditions because the lift characteristics often change considerably and even become nonlinear. Therefore, the loading for the high-aspect-ratio wing was computed by the method outlined in reference 1, using actual high-speed section data, and the results are presented for 0.40 and 0.80 Mach number in figure 1(a). This wing was particularly amenable to theoretical analysis since it had a simple plan form and an undistorted airfoil section for which high-speed section data were available. It is apparent that the theoretical and measured load distributions are in excellent agreement when compared at equal lift coefficients. The loading changes quite radically at Mach numbers of 0.85 and above. From figure 10 it may be seen that for all positive lift coefficients, the center of load of this model moves outboard above 0.77 Mach number. The shift is greatest at low angles of attack and would result in variation in trim and stability due to changes in the downwash at the tail. A further effect of this shift in the center of load is to increase the root bending moment. For a 3g pull-out the increase is 5 percent as the Mach number changes from 0.77 to 0.90. This bending moment is about 2.5 percent greater than that predicted by ANC-1(1).

The loading on the wing of model A, shown on figure 2, is quite different from that on the high-aspect-ratio wing. Part of this difference is apparently due to a substantial amount of lift

contributed by the fuselage because the loading at the wing root is too great to be accounted for by the additional area or the change in effective angle of attack caused by the small leading-edge extension at the wing root. Although there is a small increase in root bending moment due to the outward shift of the center of lift with increasing Mach number, the root bending moment never quite attains the value predicted by ANC-1(1). Since no high-speed section data were available for the airfoil used on this wing, no other theoretical calculations were attempted.

Model B (fig. 3) is another example of an airplane with a wing which departs radically from a straightforward design. In this case however, it is the unusual wing root which carries more than the expected load at high Mach numbers. The experimental results indicate tip loads lower than those computed by ANC-1(1) and for this reason the root bending moments are less than the theoretically predicted ones at nearly all lift coefficients and Mach numbers. The somewhat irregular distributions measured at the higher Mach numbers may be due to support strut interference.

Model C (fig. 4) has a wing of conventional plan form, thickness variation, and twist distribution. With increasing Mach number the lift for a given angle of attack first increases as a result of the increase in lift-curve slope. Due to its greater thickness and higher angle of attack the root section exceeds the critical Mach number first, resulting in a decrease in load carried by this section. At the higher Mach numbers all sections of the wing are operating above their critical conditions, resulting in a general decrease in loading across the span. The loss of lift at the root section causes an outward shift in the center of loading with a consequent increase in wing root bending moment. At a Mach number of 0.80 and a lift coefficient corresponding to a 3g pull-out at 5000 feet the bending-moment at the wing root is about 17 percent greater than for a similar pull-out at 0.6 Mach number.

Although the wing of model D (fig. 5) and the high-aspect-ratio wing (fig. 1) are quite similar in plan form they differ considerably in sweepback, dihedral, thickness, and twist. Also, the wing of model D was tested in combination with a fuselage. The thickness and twist distribution of the model D wing appear quite satisfactory, since the wing does not experience any large loss in lift over the root section at the higher Mach numbers. Figure 10 shows that the lateral center of lift actually shifts inboard with increasing speed.

Model E (fig. 6) is a special case, since it is the only model of the group with a wing of the inverted-gull type. The large loss of lift over the inboard section of the wing is due to the thicker inboard wing panel having the lowest critical speed and to separation of flow at the point of dihedral reversal. Figure 10 shows a continuous outward shift of the lateral center of lift as the Mach number is increased. This shift of loading results in an increase in bending moment at the wing root of approximately 15 percent above the theoretical value for a 3g pull-out at a Mach number of 0.80 and an altitude of 5000 feet.

Although rather incomplete span-load data were obtained during the model F tests, because the model had but three wing pressure stations, the data have been included because the simple and straightforward design of the wing make it amenable to theoretical treatment. While the airfoil employed is not a basic section, it is closely related to one for which high-speed section data are available. The upper sets of curves in figure 7 show the span loading at 0.40 and 0.80 Mach number as determined from wind-tunnel tests. The lower sets of curves are for the loading computed from section data by the method of reference 1, and the test points shown are from measured loadings at the same lift coefficient as the computed loadings. As no wind-tunnel data were available for the $65_{(112)}$-213 airfoil the section characteristics used in the computations were obtained by plotting available wind-tunnel data for the 65_1-series airfoils and then extrapolating to get characteristics for a 65_1-213 airfoil. The agreement between the theoretical and measured loadings is excellent at 0.40 Mach number but the loss of lift measured at the wing root is not indicated by the theoretical analysis. It is believed that this loss of lift at the root may be the result of interference between the wing and fuselage because the fuselage air-intake ducts undoubtedly have an appreciable effect upon the wing-root pressures.

CONCLUDING REMARKS

Correlation of available span-load data from high-speed wind-tunnel tests indicated that in the majority of cases the center of lift shifted outboard at the higher Mach numbers. Although this shift resulted in wing-root bending moments greater than those indicated by low-speed wind-tunnel tests, in some cases the center of lift did not shift outboard of the point computed by low-speed theory. For two of the models tested the center of lift actually shifted inboard with increasing Mach number. The excellent high-speed characteristics of the one model, which had a thickened wing

root housing an air-inlet duct, were apparently due to three-dimensional effects produced by the sweepback and taper of the root section. The other model for which the center of lift shifted inboard had a highly tapered wing of constant thickness ratio with about 2° of washout. The outboard shift of loading for a model with an inverted-gull wing was apparently due to premature separation and loss of lift at the point of dihedral reversal.

When high-speed airfoil data were available and the model wing was of conventional plan form and was not subjected to large interference effects from other parts of the model it was possible to compute the span load distribution at high Mach numbers with considerable accuracy.

Ames Aeronautical Laboratory,
National Advisory Committee for Aeronautics,
Moffett Field, Calif.

REFERENCES

1. Boshar, John: The Determination of Span Load Distribution at High Speeds by Use of High-Speed Wind-Tunnel Section Data. NACA ACR 4B22, 1944.

2. Anon.: Spanwise Air-Load Distribution, ANC-1(1). Army-Navy-Commerce Committee on Aircraft Requirements. April 1938.

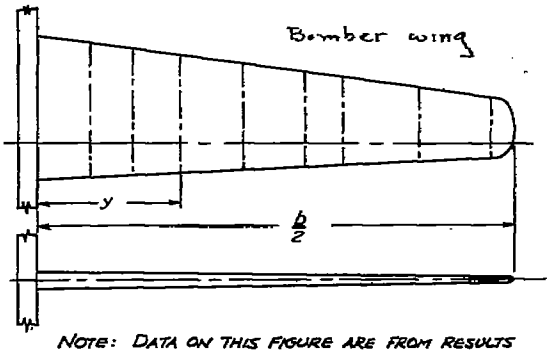

Note: Data on this figure are from results of tests in the Langley 8-foot high-speed tunnel.

Wing Dimensional Data						
2y/b	0	0.3	0.5	0.7	0.9	1.0
Airfoil section	65,-210					
Thickness, percent chord	10	10	10	10	10	10
Chord, ft.	0.500	0.410	0.350	0.290	0.230	0.200
α - chord line, deg.	0	0	0	0	0	0
S = 1.10 sq.ft.	b = 3.15 ft.		$\bar{c}$ = 0.349 ft.		A = 9.02	

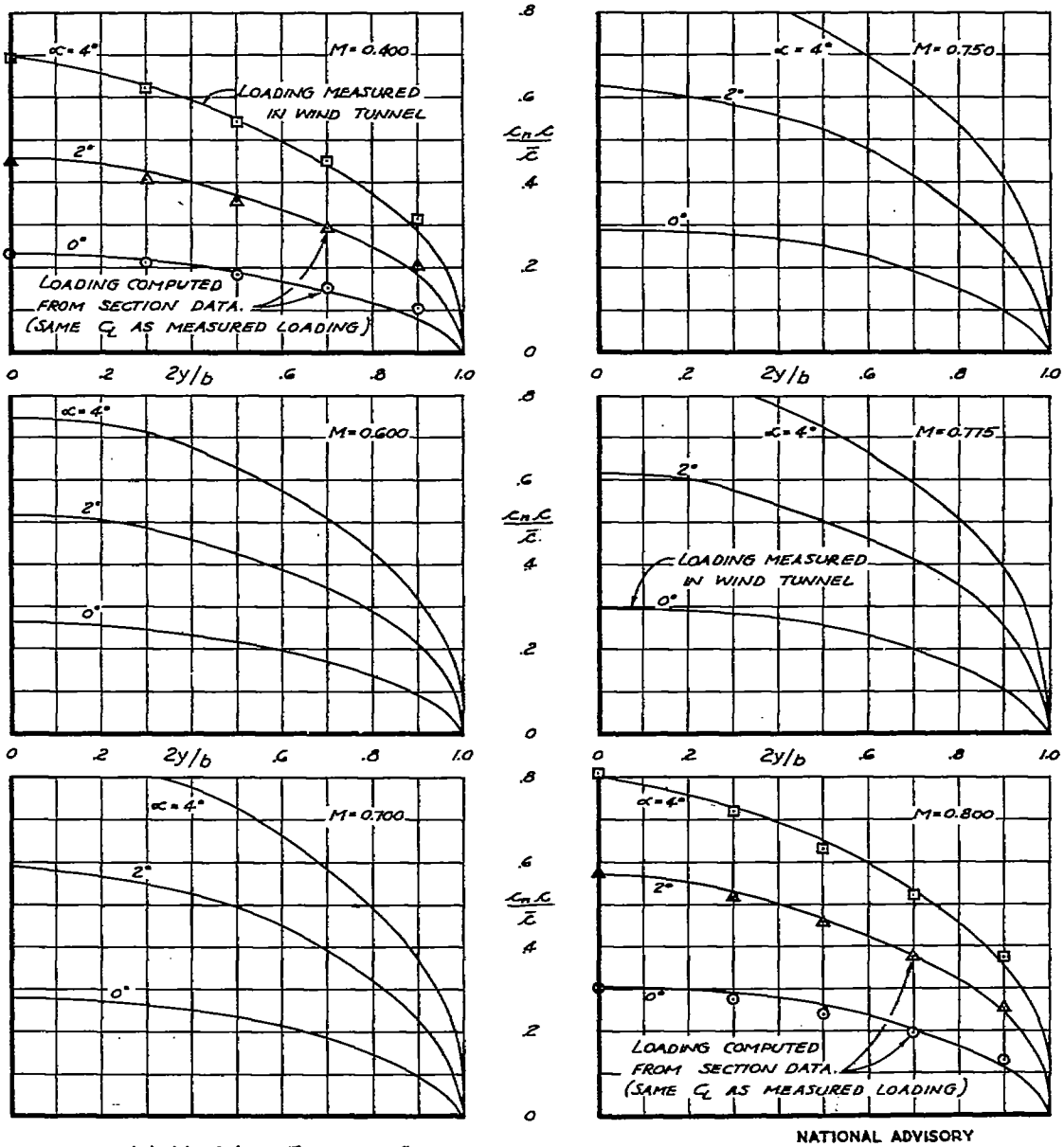

(a) M = 0.400 To M = 0.800

National Advisory Committee for Aeronautics

Figure 1.- Spanwise variation of section loading for a model of a high-aspect-ratio wing.

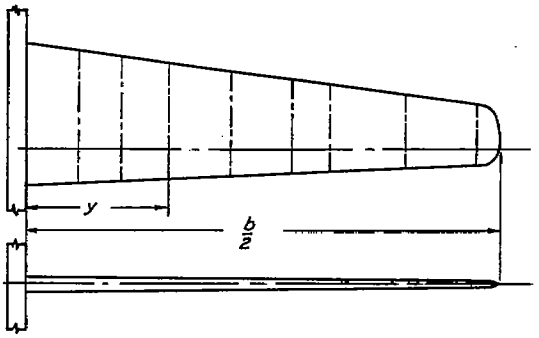

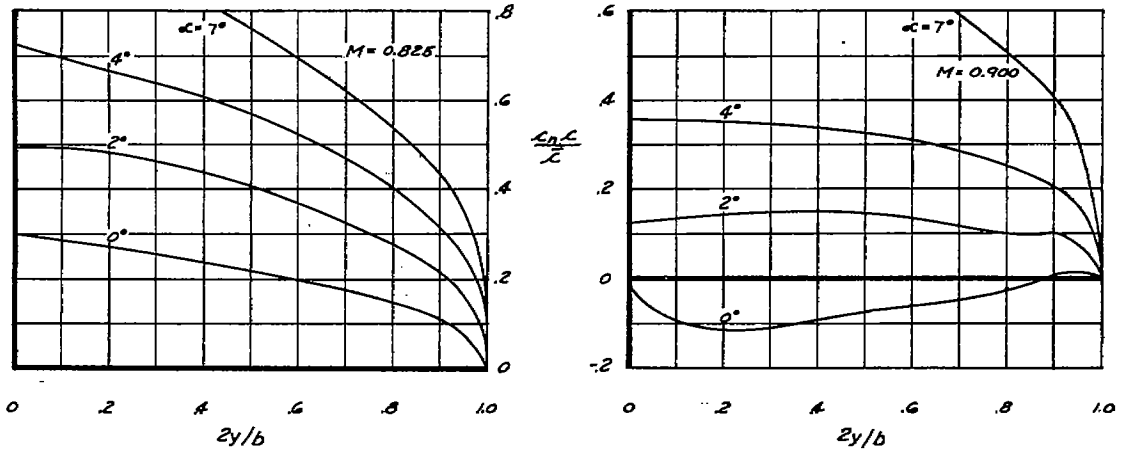

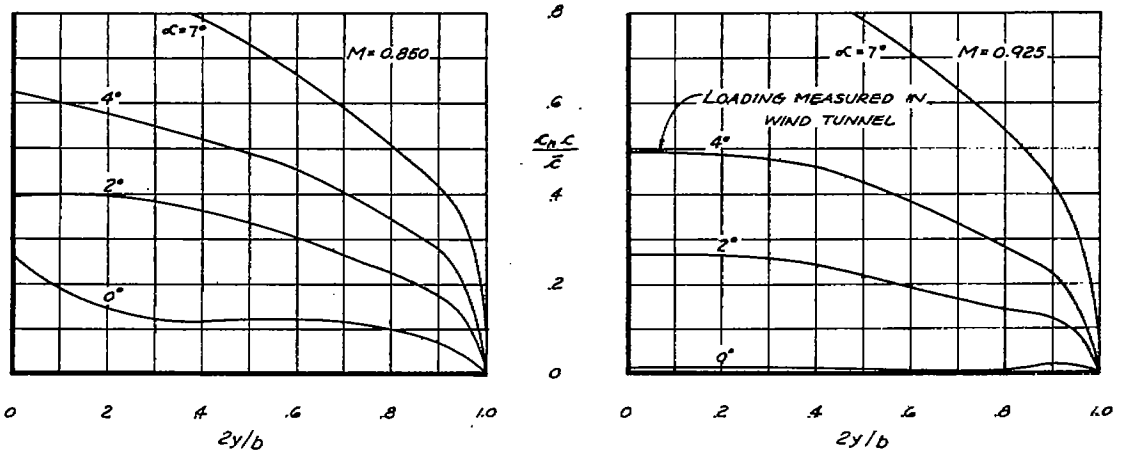

NATIONAL ADVISORY COMMITTEE FOR AERONAUTICS

(b) M = 0.825 TO M = 0.925

FIGURE 1.- CONCLUDED.

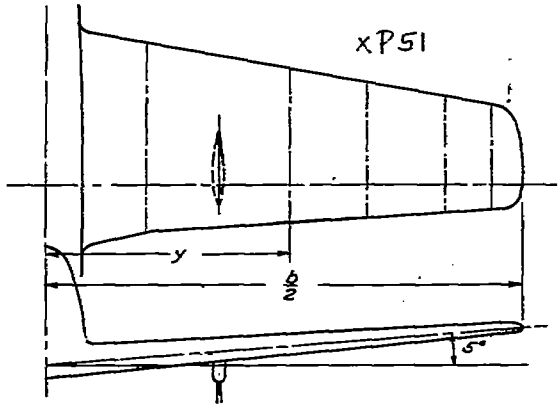

WING DIMENSIONAL DATA						
2y/b	0	0.3	0.5	0.7	0.9	1.0
AIRFOIL SECTION	NAA LOW-DRAG SECT.					
THICKNESS, PERCENT CHORD	15.07 TH. 15.00 ACT.	15.25	14.49	13.48	12.04	11.07
CHORD, FT.	2.889	2.422	2.111	1.800	1.489	1.333
α - ZERO LIFT LINE, DEG.	2.47	2.22	1.85	1.38	0.72	0.33
S = 25.91 SQ. FT.	b = 12.34 FT.		$\bar{c}$ = 2.100 FT.		A = 5.89	

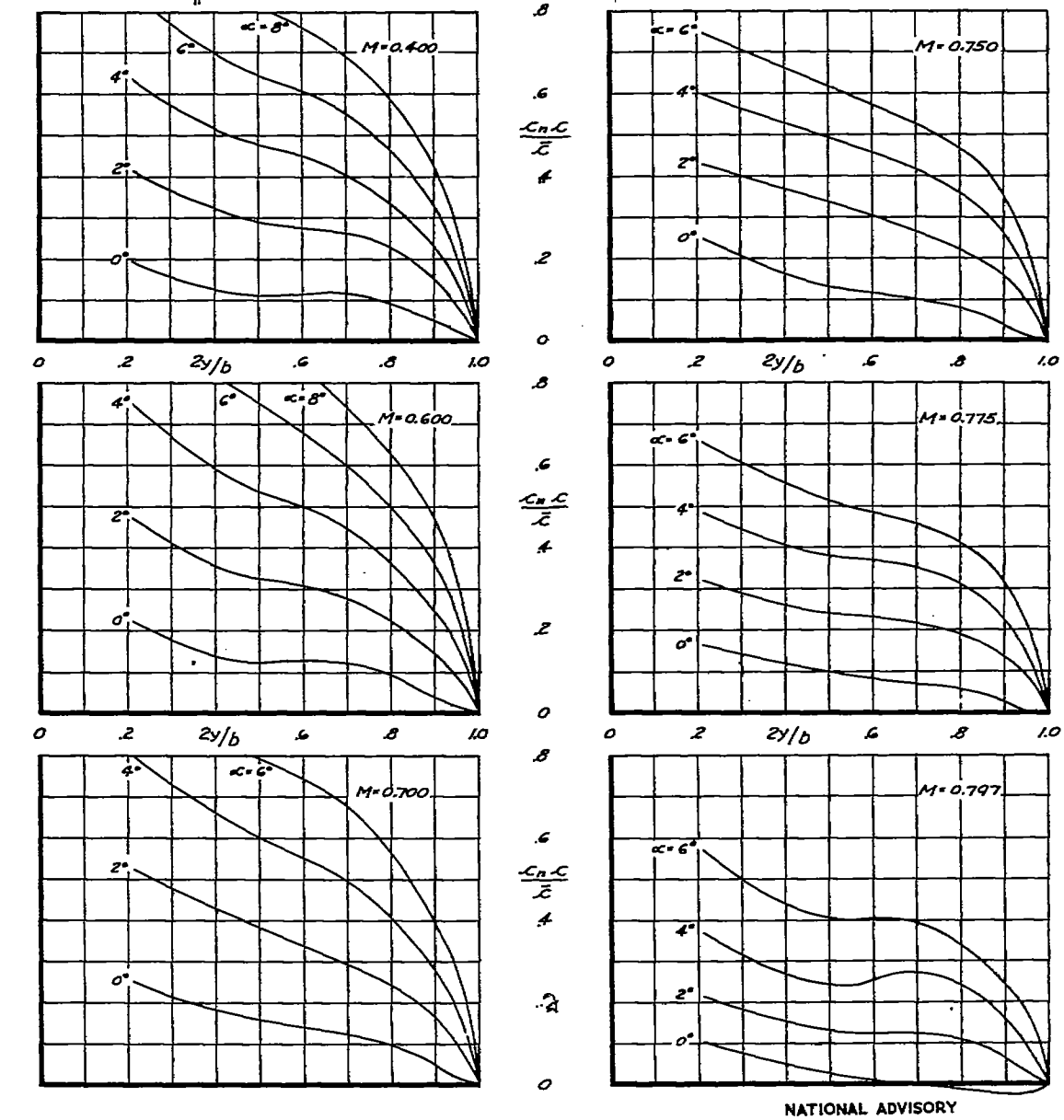

NATIONAL ADVISORY COMMITTEE FOR AERONAUTICS

FIGURE 2.- SPANWISE VARIATION OF SECTION LOADING FOR AIRPLANE MODEL A.

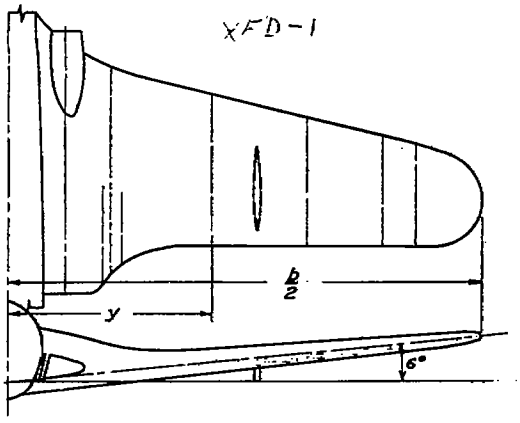

WING DIMENSIONAL DATA						
2y/b	0	0.3	0.5	0.7	0.9	1.0
AIRFOIL SECTION	NACA 66,2-218 TH. ROOT - NO FILLET ⟷				NACA 66,2-414	
THICKNESS, PERCENT CHORD	18.0 (THEO.)	17.4	16.7	16.0	14.8	14.0
CHORD, FT.	2.667 (THEO.) 2.262 2.209		1.905	1.600	1.295	1.143
α - CHORD LINE, DEG.	0					-2.0
S = 22.551 SQ.FT.	b = 12.000 FT.		$\bar{c}$ = 1.879 FT.		A = 6.40	

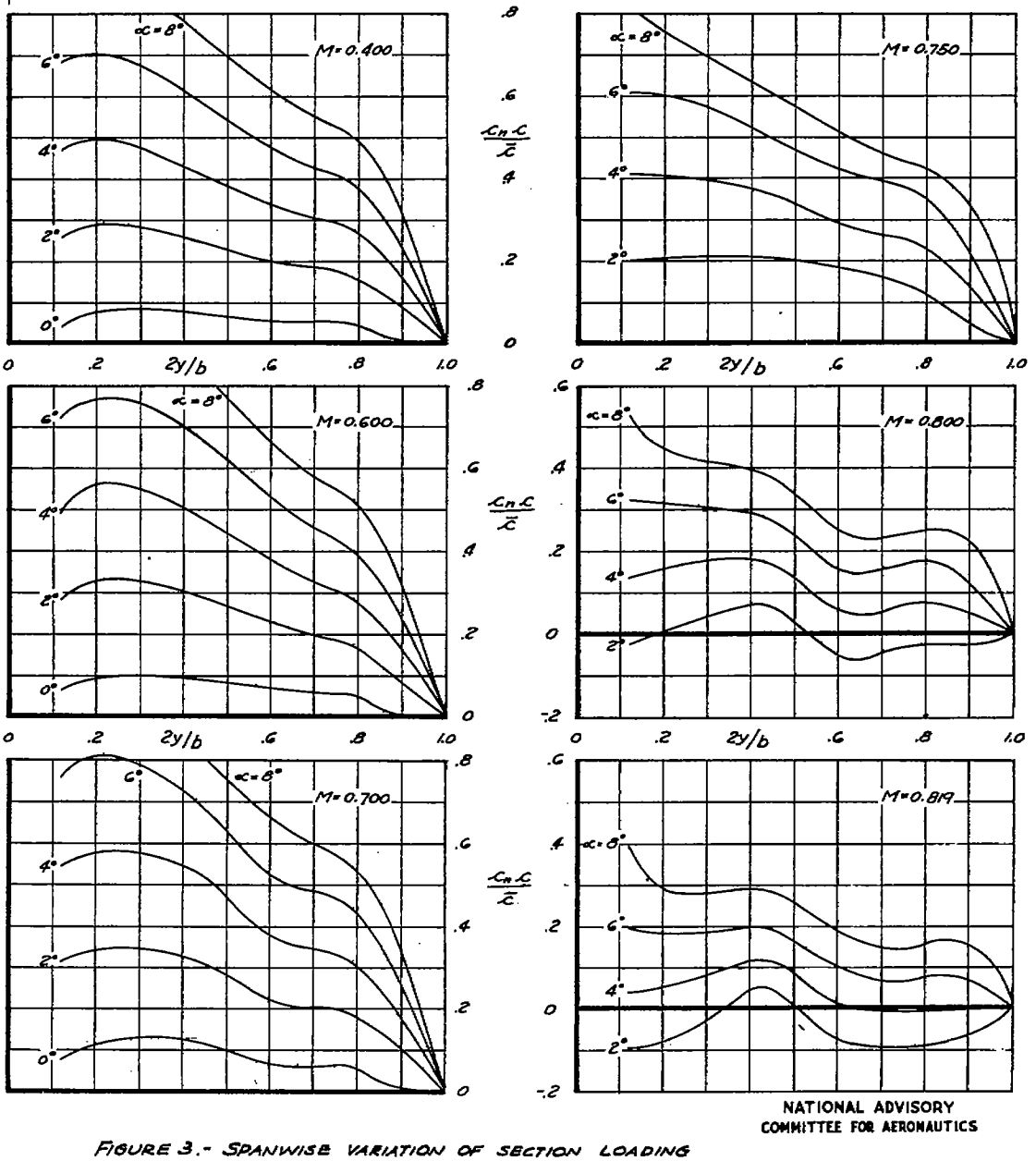

NATIONAL ADVISORY COMMITTEE FOR AERONAUTICS

FIGURE 3.- SPANWISE VARIATION OF SECTION LOADING FOR AIRPLANE MODEL B.

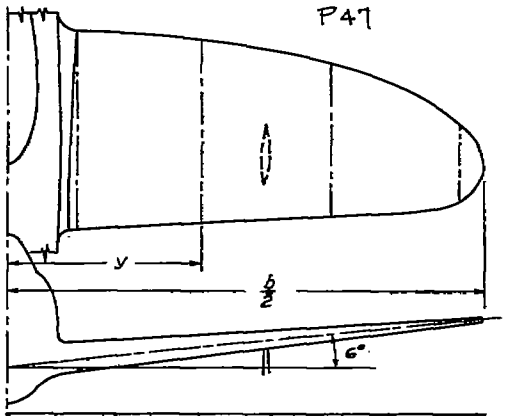

WING DIMENSIONAL DATA						
2y/b	0	0.3	0.5	0.7	0.9	1.0
AIRFOIL SECTION	REPUBLIC S-3					
THICKNESS, PERCENT CHORD	15.0	14.2	12.3	10.5	9.2	9.0
CHORD, FT.	2.746	2.577	2.358	2033	1.362	0
α - CHORD LINE - DEG.	1.00	1.00	0.90	-0.05	-1.96	-2.96
S = 27.00 SQ.FT.	b = 12.233 FT.		$\bar{c}$ = 2.207 FT.		A = 5.96	

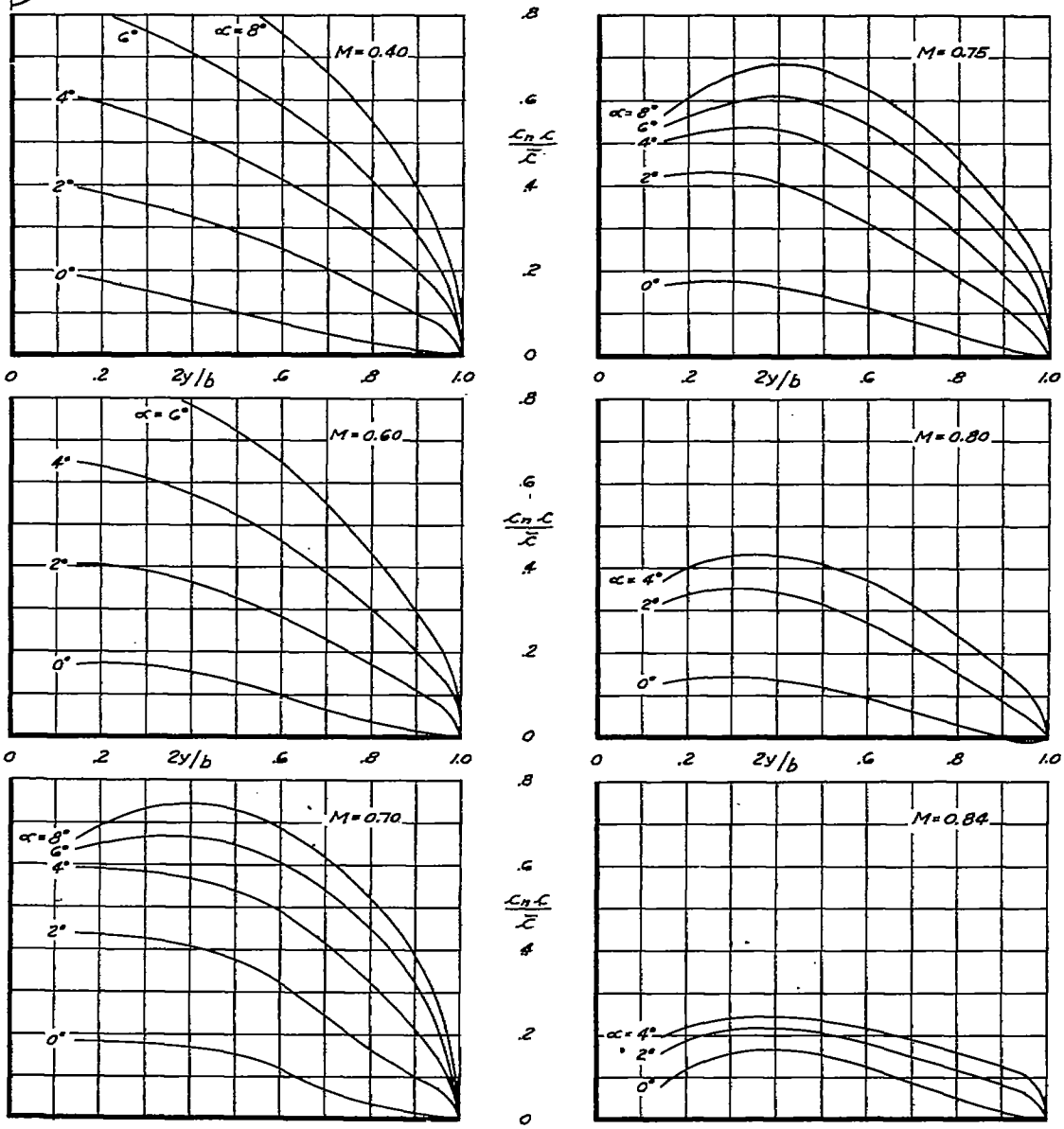

NATIONAL ADVISORY COMMITTEE FOR AERONAUTICS

FIGURE 4.- SPANWISE VARIATION OF SECTION LOADING FOR AIRPLANE MODEL C.

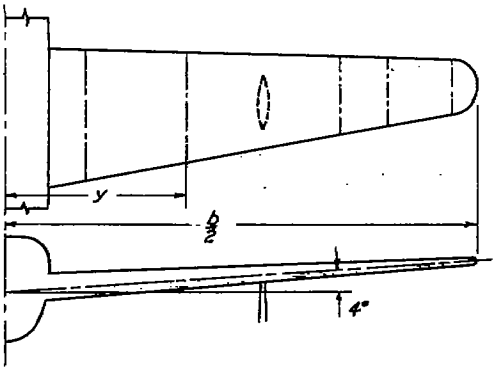

Wing Dimensional Data						
2y/b	0	0.3	0.5	0.7	0.9	1.0
Airfoil Section	Douglas G-17					
Thickness, Percent Chord	17.02	17.02	17.02	17.02	17.02	17.02
Chord, Ft.	2.084	1.666	1.387	1.108	0.830	0.690
α - Chord Line, Deg.	-2.00	-2.26	-2.51	-2.90	-3.54	-4.06
S = 17.23 Sq.Ft.	b = 12.46 Ft.		$\bar{c}$ = 1.383 Ft.		A = 9.00	

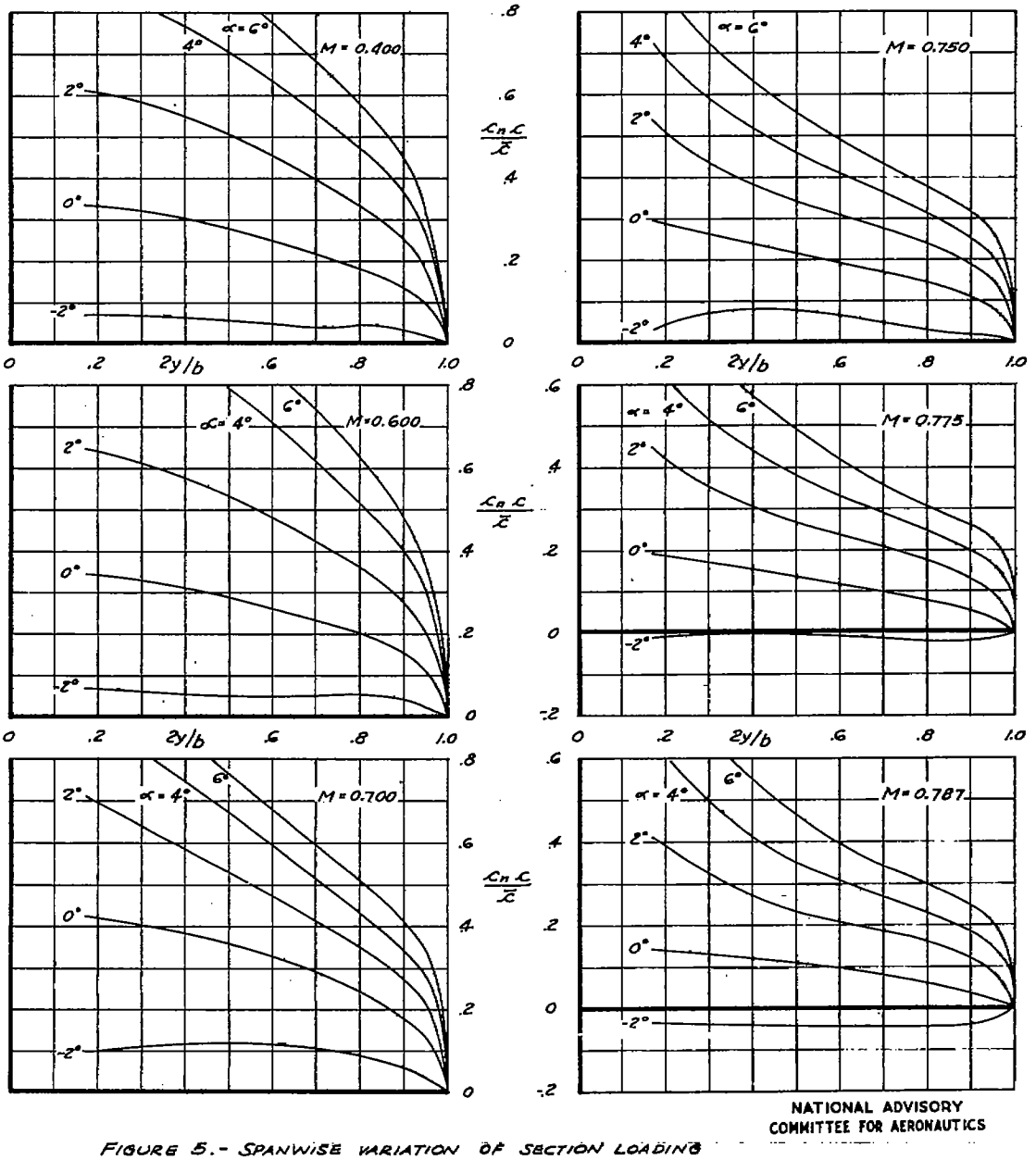

NATIONAL ADVISORY COMMITTEE FOR AERONAUTICS

FIGURE 5.- SPANWISE VARIATION OF SECTION LOADING FOR AIRPLANE MODEL D.

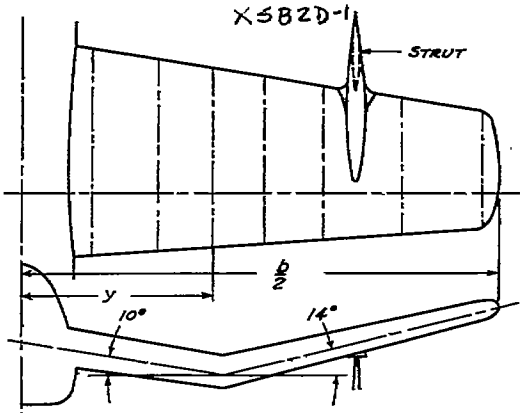

WING DIMENSIONAL DATA						
2y/b	0	0.3	0.5	0.7	0.9	1.0
AIRFOIL SECTION	DOUGLAS ESXX25-218 AT ROOT		NACA 65,2-2518,0-0.5 AT 2y/b = 0.419		NACA 65,2-2515 0-0.5 AT TIP	
THICKNESS, PERCENT CHORD	18.00	18.00	17.72	16.88	15.74	15.00
CHORD, FT.	2094	1.785	1.570	1.361	1.151	1.047
α- CHORD LINE, DEG.	2.00	2.00	2.00	2.00	2.00	2.00
S = 13.18 SQ.FT.	b = 8.435 FT.		$\bar{c}$ = 1.562 FT.		A = 5.40	

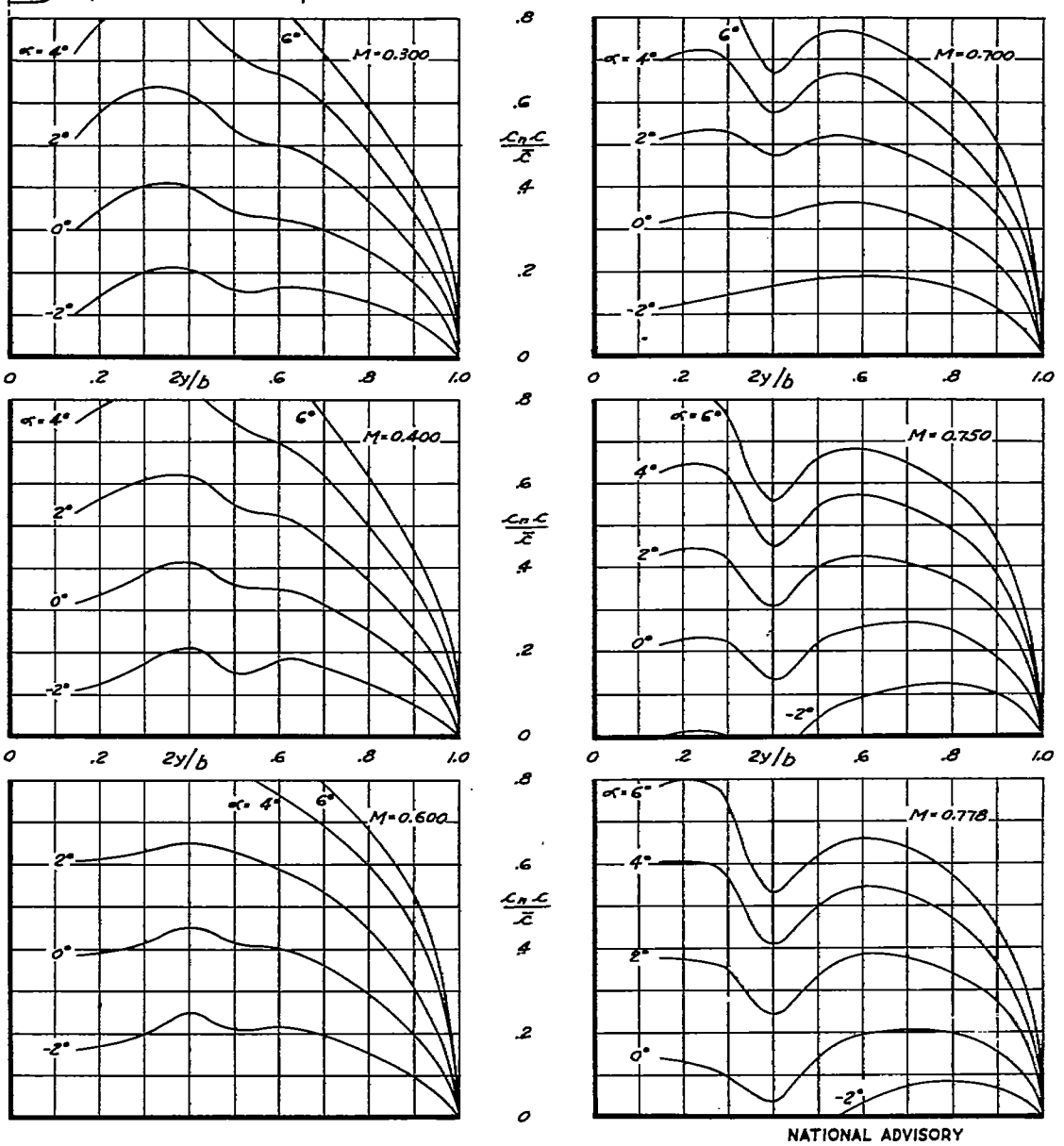

NATIONAL ADVISORY COMMITTEE FOR AERONAUTICS

FIGURE 6.- SPANWISE VARIATION OF SECTION LOADING FOR AIRPLANE MODEL E.

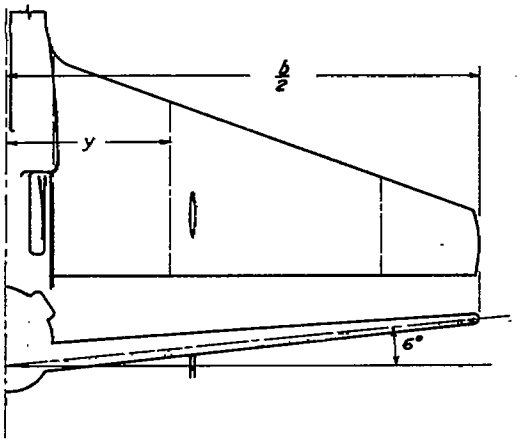

WING DIMENSIONAL DATA						
$2y/b$	0	0.3	0.5	0.7	0.9	1.0
AIRFOIL SECTION	65(112)-213					
THICKNESS, PERCENT CHORD	13	13	13	13	13	13
CHORD, FT.	3.271	2.671	2.104	1.637	1.171	0.938
α - CHORD LINE, DEG.	2.5	2.5	2.5	2.5	2.5	2.5
$S = 26.53$ SQ. FT.	$b = 12.59$ FT.		$\bar{c} = 2.104$ FT.		$A = 5.98$	

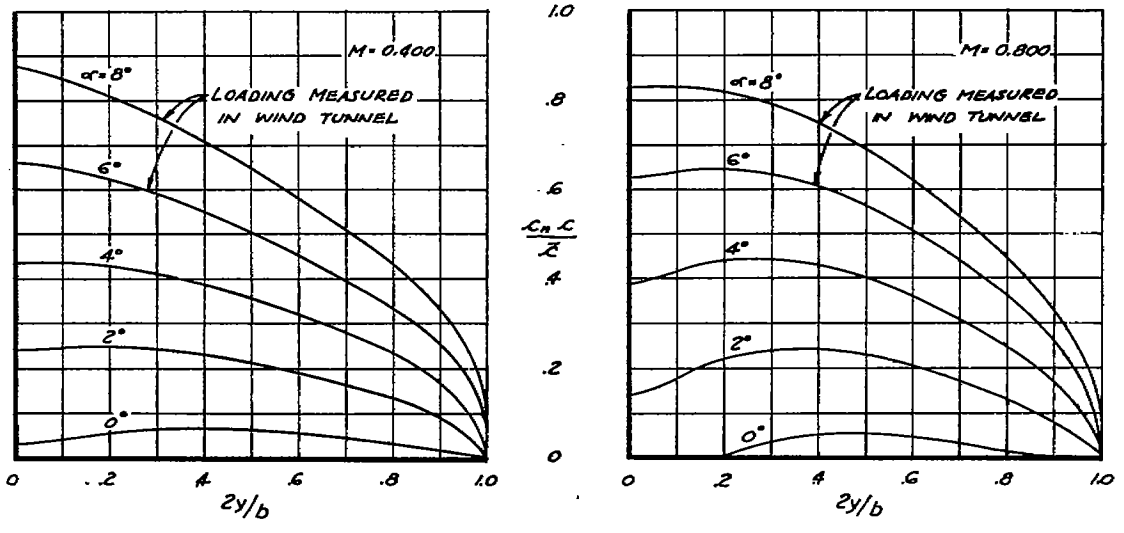

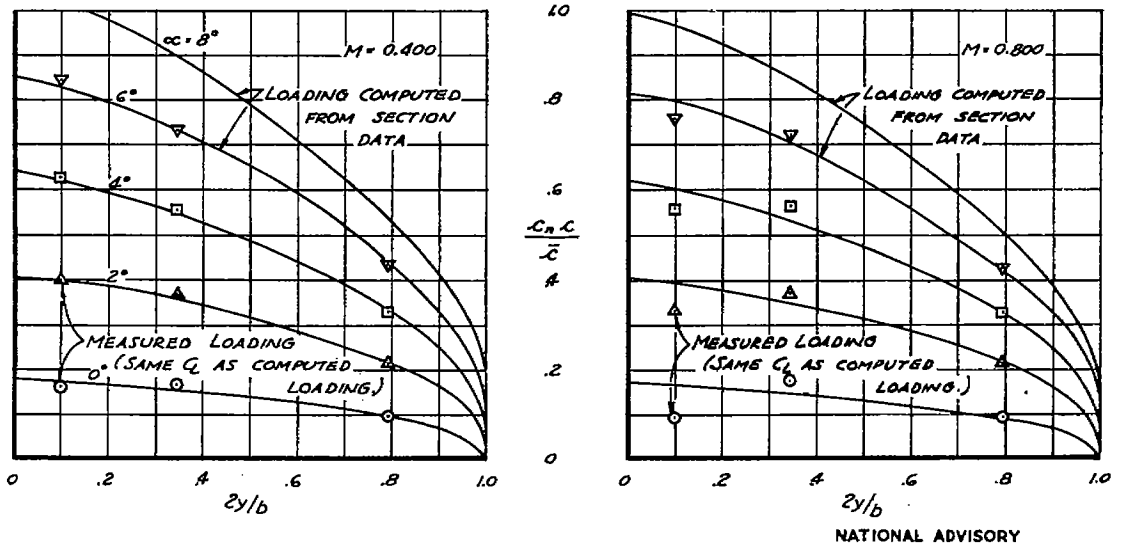

NATIONAL ADVISORY COMMITTEE FOR AERONAUTICS

FIGURE 7.- SPANWISE VARIATION OF SECTION LOADING FOR AIRPLANE MODEL F.

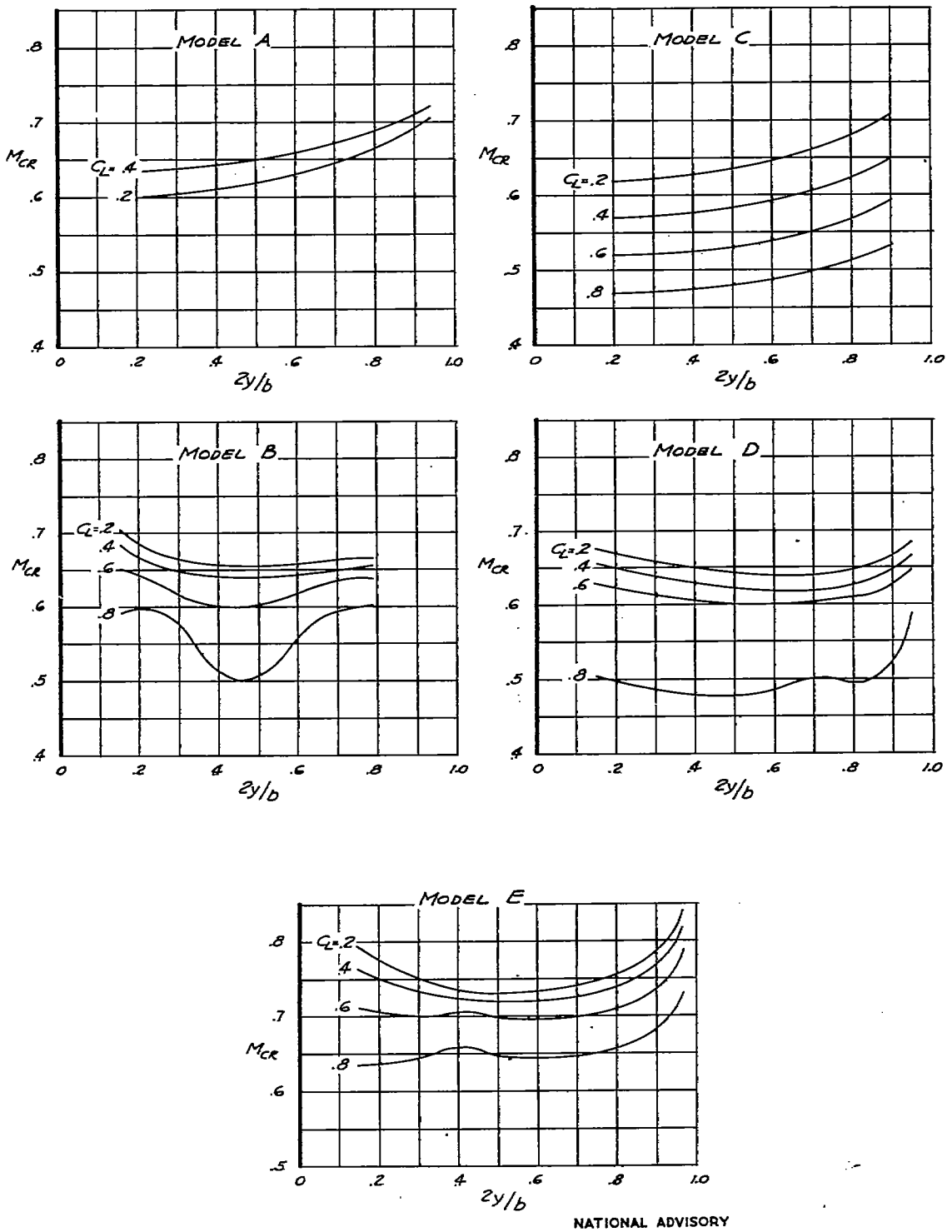

FIGURE 8.- SPANWISE VARIATION OF CRITICAL MACH NUMBER FOR MODELS OF SEVERAL AIRPLANES.

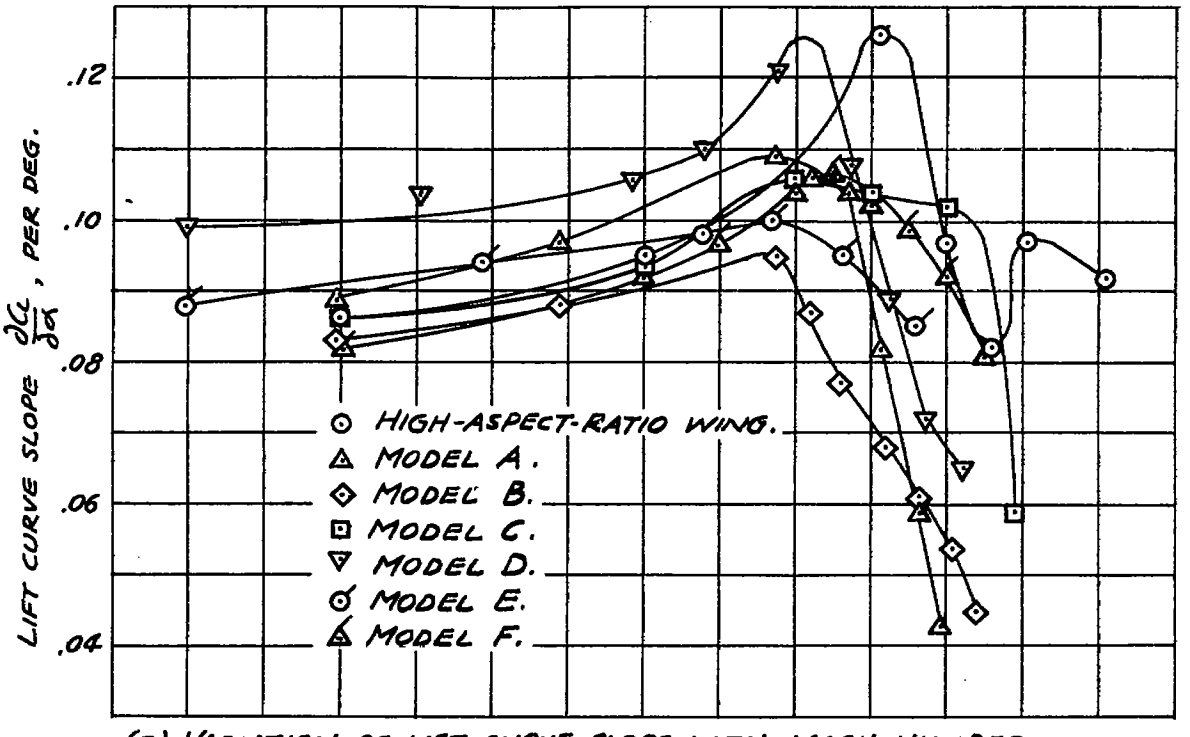

(a) VARIATION OF LIFT-CURVE SLOPE WITH MACH NUMBER.

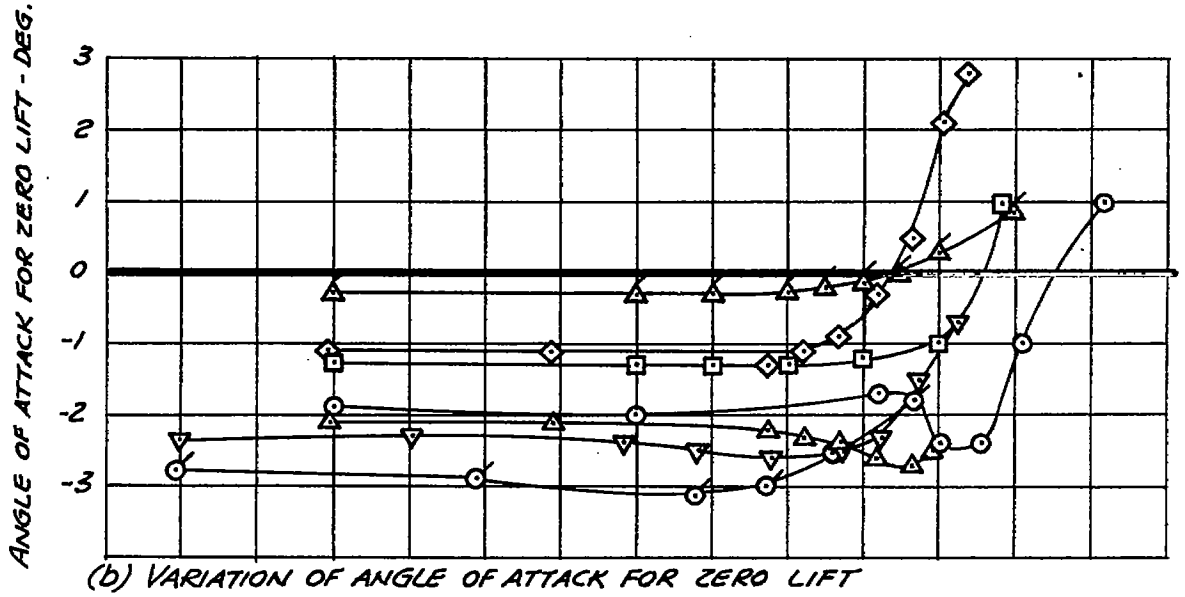

(b) VARIATION OF ANGLE OF ATTACK FOR ZERO LIFT WITH MACH NUMBER

NATIONAL ADVISORY COMMITTEE FOR AERONAUTICS

FIGURE 9.- VARIATION OF LIFT CHARACTERISTICS WITH MACH NUMBER FOR MODELS OF SEVERAL AIRPLANES.

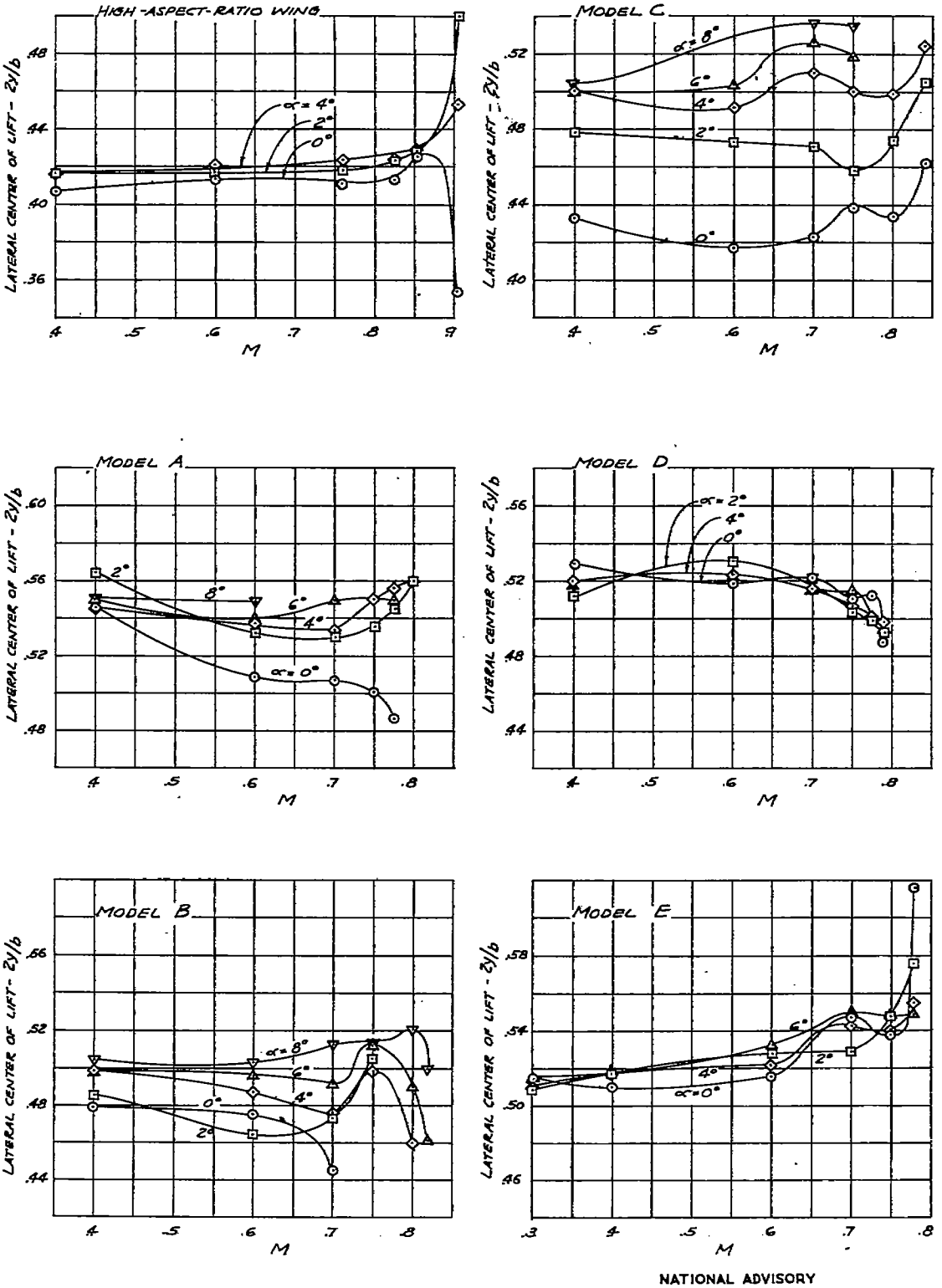

NATIONAL ADVISORY
COMMITTEE FOR AERONAUTICS

FIGURE 10.- VARIATION OF LATERAL CENTER OF LIFT WITH MACH NUMBER FOR MODELS OF SEVERAL AIRPLANES.